



## Full Length Article

# Excellent electrochemical stability of graphite nanosheet-based interlayer for electric double layer capacitors

Geon-Hyoung An<sup>a</sup>, Hyo-Jin Ahn<sup>a,b,\*</sup>

<sup>a</sup> Program of Materials Science & Engineering, Convergence Institute of Biomedical Engineering and Biomaterials, Seoul National University of Science and Technology, Seoul 01811, Republic of Korea

<sup>b</sup> Department of Materials Science and Engineering, Seoul National University of Science and Technology, Seoul 01811, Republic of Korea



## ARTICLE INFO

## Keywords:

Interface engineering  
Electric double layer capacitors  
Current collector  
Graphene  
Electrochemical stability

## ABSTRACT

Characterized by high power density and long cycle life, electric double layer capacitors have been considered to be most promising energy storage devices. However, the use of low electrolyte concentration due to the degradation of current collector in high electrolyte concentration involves their limitation for ionic diffusion at high current densities during cycling, leading to a low electrochemical behavior. Therefore, the sensible design of the interfacial structure between the current collector and the active material is a supreme technology for accomplishing desired requirements as the improved performance of current collector. In the present paper, by applying the graphite nanosheet as an interlayer on the nickel (Ni) current collector, the electrochemical performance is improved with high specific capacitance ( $236 \text{ F g}^{-1}$  at the current density of  $0.2 \text{ A g}^{-1}$ ), outstanding high-rate ability (87%), and excellent cycling stability (93% after 10,000 cycles in the high-concentration electrolyte). Hence, the advantages of this unique approach include the improvement of the contact area between the current collector and the active material and prevention of the oxidation of the Ni current collector. This enhanced electrochemical performance suggests that this interface engineering is a powerful strategy for potential applications in electric double layer capacitors.

## 1. Introduction

Owing to the characteristics such as high-power density, long cycle stability, and wide range of operating temperature [1–4], electrochemical capacitors have been extensively studied in recent years to meet the many emerging applications such as transportation, backup system, and regenerative braking. Electrochemical capacitors can be typically categorized into ultracapacitors related to the electrical double-layer and supercapacitors using the electroactive species diffuses into and out of the interior of the crystal structure of the solid electrode. In general, the ultracapacitors as electric double layer capacitors (EDLCs) consist of both electrodes using activated carbon on a current-collector and the electrolyte. Due to its high surface area, high electrical conductivity, and excellent chemical stability [5–8], activated carbon has consistently proved to be a powerful candidate as an active material. However, almost research effort has focused on activated carbon related to the high surface area, mesoporous volume fraction, and electrical conductivity itself, rather than on the current collector and the electrolyte [9–16].

Hence, to further improve the energy storage performance of EDLCs, a careful consideration of interface engineering between the current collector and activated carbon is needed in order to improve electrical property, chemical stability, and ionic diffusion transport [17–20]. In addition, in terms of maximizing the effectiveness of interface engineering, the use of high-concentration electrolytes is highly attractive due to the large number of working ions during the cycling, which leads to the improved capacitance at high current densities. However, the use of potassium hydroxide (KOH)-based aqueous electrolytes with a high ionic conductivity as the typical electrolyte for EDLCs causes the corrosion of the current collector in high-concentration, leading to a poor cycling stability of EDLCs [3,9,11]. Nevertheless, the interface engineering between the current collector and activated carbon has received relatively little attention thus far.

To fill this gap, in the present study, we design a graphite nanosheet and apply it as an efficient interlayer between the current collector and activated carbon for EDLCs by a high-concentration electrolyte from the perspective of the following potential advantages: (1) the graphite nanosheet with an excellent chemical stability can act as an effective

\* Corresponding author at: Department of Materials Science and Engineering, Seoul National University of Science and Technology, Seoul 139-743, Republic of Korea.

E-mail address: [hjahn@seoultech.ac.kr](mailto:hjahn@seoultech.ac.kr) (H.-J. Ahn).

<https://doi.org/10.1016/j.apsusc.2018.12.120>

Received 20 July 2018; Received in revised form 7 November 2018; Accepted 12 December 2018

Available online 13 December 2018

0169-4332/ © 2018 Elsevier B.V. All rights reserved.

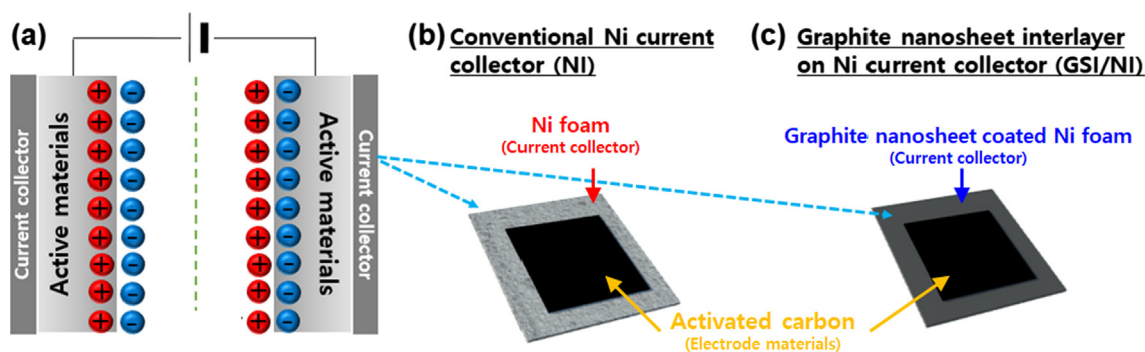


Fig. 1. Schematic illustration for (a) components of electrical double layer capacitors (EDLCs); (b) conventional Ni current collector (NI), and (c) graphite nanosheet interlayer on the Ni current collector (GSI/NI).

barrier to prevent corrosion of the current collector from the high-concentration electrolyte; (2) the roughly two dimensional structures of the graphite nanosheet on the current collector can provide a large contact area between the current collector and activated carbon, therefore promoting a favorable electrical contact at high current densities. The graphite nanosheet was used as an efficient interlayer on the current collector due to its outstanding electrical, chemical, and mechanical properties, all of which can permit nano-scale engineering for interlayers to achieve excellent chemical stability and to enhance the electrical property.

## 2. Results and discussion

Fig. 1a shows the components and reaction mechanism of EDLCs. The electrodes of EDLC consist of the current collector and an active material in an electrolyte. The separation of charge occurs on polarization at the activated carbon and electrolyte interface. During the discharging process, the created electrons transfer through the current collector and the external circuit connecting both electrodes. In previous research, the conventional Ni foam (NI) was typically used for the current collector (see Fig. 1b). In this study, we suggest a novel design of the graphite nanosheet as an interlayer on the Ni foam (GSI/NI) (see Fig. 1c) by the dip-coating process.

To obtain the high electrical double layer area, the commercial activated carbon with a high surface area ( $2400 \text{ m}^2 \text{ g}^{-1}$ , see Table S1) was used as an active material coated on the current collector (see Figs. S1 and S2). Fig. 2 shows the graphite nanosheet for the use in interface engineering between the current collector and activated carbon. The scanning electron microscopy (SEM) image of graphite nanosheet showed the average size of 5 to  $7 \mu\text{m}$  (see Fig. 2a). In addition, the dip-coating process (E-flex, Nano Dip Coater, EF-7100) including automatic systems was enough for the uniform coverage of the interlayer on the surface of the Ni collector see Fig. S3. Fig. 2b shows typical tapping-mode atomic force microscope (AFM) results of the graphite nanosheet onto a silicon dioxide substrate, implying the layered graphene structures (see Fig. 2b). The topographic height profile of the graphite nanosheet presents the edge of thin graphene layers with a step of  $\sim 7.9 \text{ nm}$ , suggesting the multilayered graphene structure with ca. 23 layers. In addition, the transmission electron microscopy (TEM, Gwangju Center, Korea Basic Science Institute) was performed to examine the nanostructural properties of the graphite nanosheet. Fig. 2c-d shows low- and high-magnification TEM images of the graphite nanosheet. The graphite nanosheet showed a clear two-dimensional structure with lattice fringes with the spacing of  $0.34 \text{ nm}$ , corresponding to the (0 0 2) plane of carbon [21,22].

Fig. 3a-b shows the low- and high-magnification SEM images of NI with a flat surface. On the other hand, GSI/NI (see Fig. 3c and d) displays a bumpy surface. In the high-magnification SEM image, the graphite nanosheet is clearly observed, implying a successful encapsulation of the Ni foam. Fig. 3e shows the X-ray diffraction (XRD) data of NI and

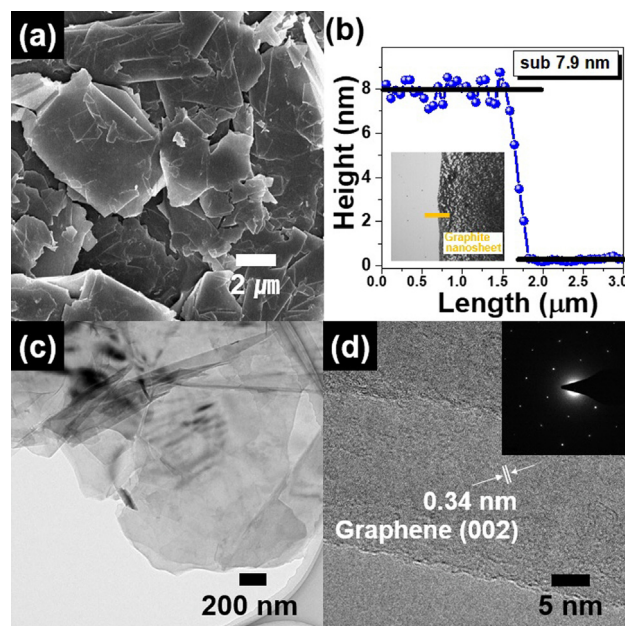


Fig. 2. (a) The SEM image of graphite nanosheet; (b) the corresponding line scan across the edge of the graphite nanosheet transferred on a silicon dioxide substrate [the inset shows the high-resolution AFM image of graphite nanosheet]; (c) low-resolution and (d) high-resolution TEM images of graphite nanosheet.

GSI/NI conducted to investigate the crystal features. All current collectors presented diffraction peaks at  $44.5^\circ$ ,  $51.8^\circ$  and  $76.4^\circ$  corresponding to the (1 1 1), (2 0 0), and (2 2 0) planes of Ni. For comparison, the diffraction peak of GSI/NI was observed at  $26.3^\circ$ , corresponding to the (1 1 1) plane. Furthermore, to confirm the uniformity of graphene layers for GSI/NI, Raman spectroscopy was performed (see Fig. 3f). Raman spectra of NI exhibited no peaks. On the other hand, GSI/NI indicated two dominant peaks at around  $1576$  and  $2686 \text{ cm}^{-1}$ , corresponding to the G and 2D mode, respectively, which are the typical aspects of a graphene structure [23–27]. In addition, for GSI/NI, the intensity ratio of the 2D to G peaks ( $I_{2D}/I_G$ ) was 0.51, revealing the typical features of a multilayered graphene structure. Based on the structural and chemical results of GSI/NI, we conclude that the graphite nanosheet consisting of a multilayered graphene structure was successfully developed on the Ni foam. Consequently, it can be expected that due to its durability against high concentration electrolyte, large contact area between the current collector and activated carbon, and strong interfacial adhesion, the graphite nanosheet on current collectors as an interlayer will considerably enhance the electrochemical performance during cycling.

Fig. 4a and b shows AFM results of NI and GSI/NI. The root mean

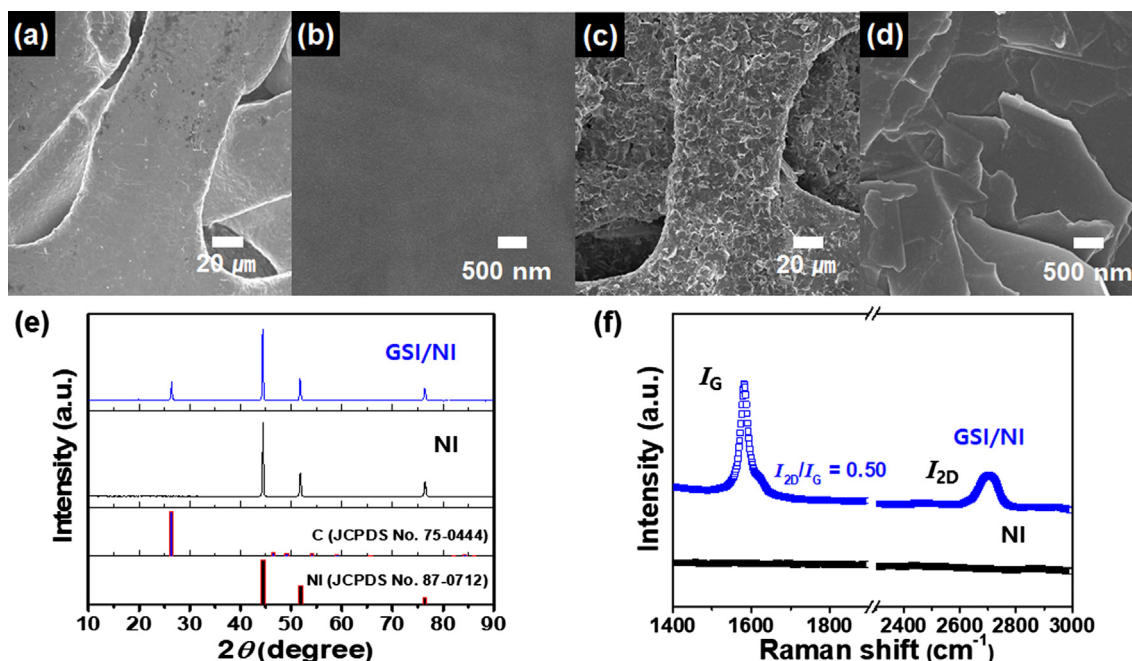


Fig. 3. (a) Low-resolution and (b) high-resolution SEM images of NI; (c) low-resolution and (d) high-resolution SEM images of GSI/NI; (e) the XRD patterns and (f) the Raman spectrum of NI and GSI/NI.

square of roughness for NI and GSI/NI was found to be 76 and 551 nm. This implies that GSI/NI has the roughest surface compared to the NI. In addition, it was found that GSI/NI has the higher surface area of  $485 \mu\text{m}^2$  compared with NI ( $406 \mu\text{m}^2$ ). Based on the AFM results, we further prove that the graphite nanosheet as an interlayer was successfully coated by a dip-coating process. Thus, it is suggested that GSI/NI with the rough surface and high surface area will significantly increase the contact area between the activated carbon and the collector, leading to improved electrochemical performance [28–30].

The interface between the current collector and activated carbon would play a significant role in enhancing the electrochemical performance of EDLCs. Therefore, to better comprehend the electrochemical kinetic feature of NI and GSI/NI, the electrochemical impedance spectroscopy (EIS) analysis (an influential measurement to inspect the interface behavior) were performed in the frequency range of  $10^2$ – $10^{-2}$  Hz. Fig. 5a and b shows the Nyquist plots of NI and GSI/NI in 6 M KOH electrolyte as the conventional solution. The semicircle in the high-frequency is ascribed to the charge transfer impedance ( $R_{ct}$ ) between the electrolyte and electrode, and the inclined line in the low-frequency corresponds with the ion diffusion in the electrodes (called the Warburg impedance). It can be seen that the  $R_{ct}$  of GSI/NI ( $0.6 \Omega$ ) is markedly low as compared to the NI ( $1.0 \Omega$ ), indicating that the

existence of the graphite nanosheet as an interlayer could enhance the electrical contact by a large contact area between the current collector and activated carbon from the rough surface. Furthermore, in the high-concentration of the 8 M KOH electrolyte (see Fig. 5c and d), in contrast to the performance in the 6 M KOH electrolyte, NI and GSI/NI showed the straight sloping line in the low frequency region, suggesting that the reduced Warburg impedance is related to a favorable ion diffusion [21,22]. These results suggest that high-concentration electrolyte in EDLCs is advantageous in terms of improving the electrochemical performance related to ionic diffusion.

To further examine the interfacial effects of energy storage performance of EDLCs, we executed the electrochemical behaviors of a full-cell system using a commercial activated carbon as a typical active material for EDLCs. However, the limited electrolyte concentration as the 6 M KOH solution is still significant drawback resulting from corrosion of the current collector and unnecessary interfacial reactions, which leads to a rapid capacitance fading. To investigate the energy storage performance of EDLCs by NI and GSI/NI, respectively, in the typical 6 M KOH electrolyte with potential range from 0.0 to 1.0 V, the specific capacitance was obtained at the current density range from 0.2 to  $20.0 \text{ A g}^{-1}$  (see Fig. 6a). The graphite nanosheet as an interlayer showed low specific capacitances, implying the little contribution for

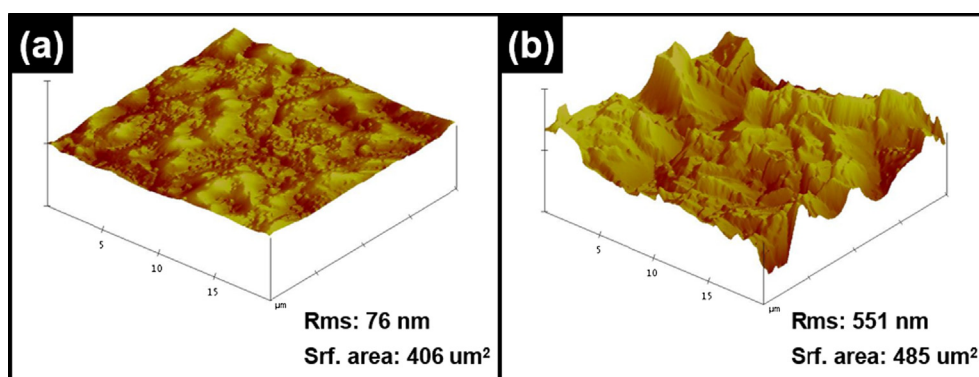


Fig. 4. AFM results of (a) NI and (b) GSI/NI.

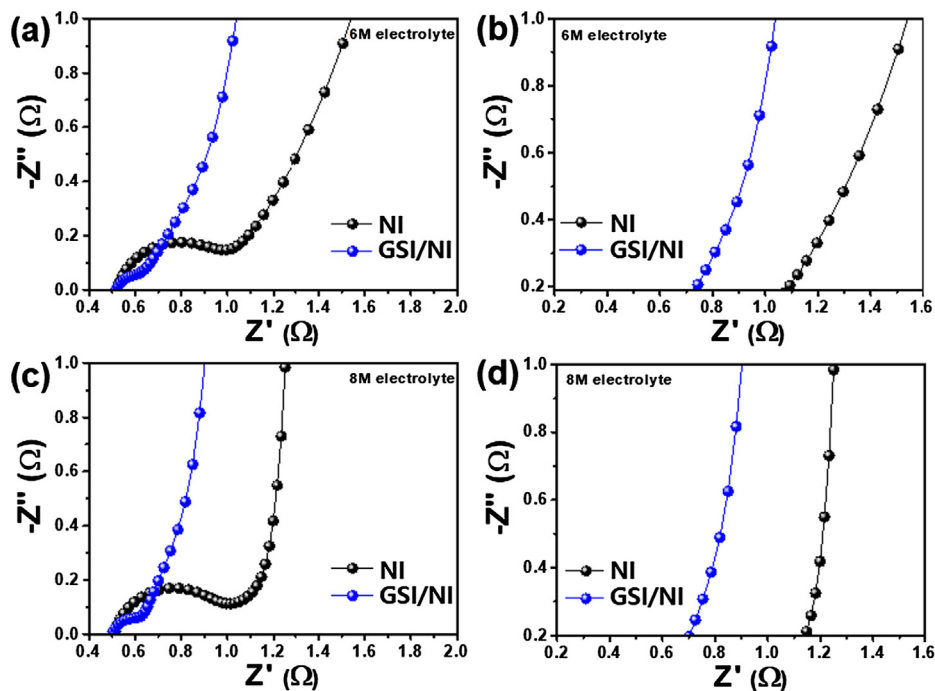


Fig. 5. Nyquist plots of (a and b) NI and (c and d) GSI/Ni in the frequency range of  $10^5$ – $10^{-2}$  Hz.

the energy storage (see Fig. S4). At the current density of  $0.2 \text{ A g}^{-1}$ , the specific capacitances of NI and GSI/Ni were amounted to 209 and  $235 \text{ F g}^{-1}$ , respectively. In addition, GSI/Ni showed higher specific capacitances than NI in all range of current density. Taken together, these results indicate that a large contact area between the current collector and activated carbon resulting in the graphite nanosheet as interlayer could considerably enhance the electrochemical performance by improved electrical contact. Furthermore, in the high-concentration of the 8 M KOH electrolyte (see Fig. 6b), the specific capacitances were also obtained. In the low current densities, the specific capacitance of GSI/Ni was  $236 \text{ F g}^{-1}$  at the current density of  $0.2 \text{ A g}^{-1}$ , which is similar to performance in the 6 M KOH electrolyte. Meanwhile, in high current densities, NI and GSI/Ni presented the enhanced high-rate ability of 78 and 87%, respectively, as compared to the performance of

NI (52%) and GSI/Ni (76%) in the 6 KOH electrolyte. The improved high-rate ability of EDLCs can mainly be attributed to the high-concentration electrolyte with the increased number of working ions during the cycling. In addition, the enhanced performance of GSI/Ni might be ascribed to the well-encapsulated graphite nanosheet, which contributes to the energy storage performance by a large contact area between the current collector and activated carbon during the cycling. In addition, the concentration electrolyte was optimized to the 8 M KOH electrolyte (see Fig. S5). As shown in Fig. 6c, GSI/Ni exhibited a rectangular curve, signifying the ideal presence of the electrical double-layer region on the surface of activated carbon [24,25]. Moreover, the rectangular curves obviously preserved their original aspects with an increase of current densities, implying an ideal energy storage. To further investigate how the graphite nanosheet as interlayer influences

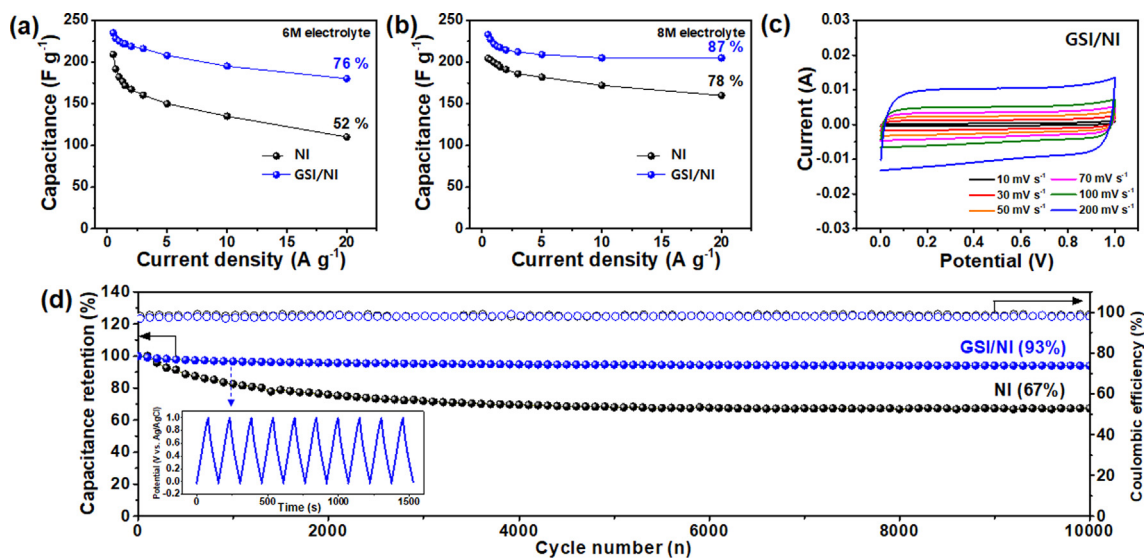


Fig. 6. Calculated specific capacitances of NI and GSI/Ni at current densities in the range  $0.2$ – $20.0 \text{ A g}^{-1}$  in the potential range  $0.0$ – $1.0 \text{ V}$  within (a) the 6 M KOH electrolyte and (b) the 8 M KOH electrolyte; (c) the CV curves of GSI/Ni at the scan rate of  $10 \text{ mV s}^{-1}$  in the potential range  $0.0$  to  $1.0 \text{ V}$ ; (d) cycling stability at the current density of  $1 \text{ A g}^{-1}$  over 10,000 cycles in 8 M KOH electrolyte.

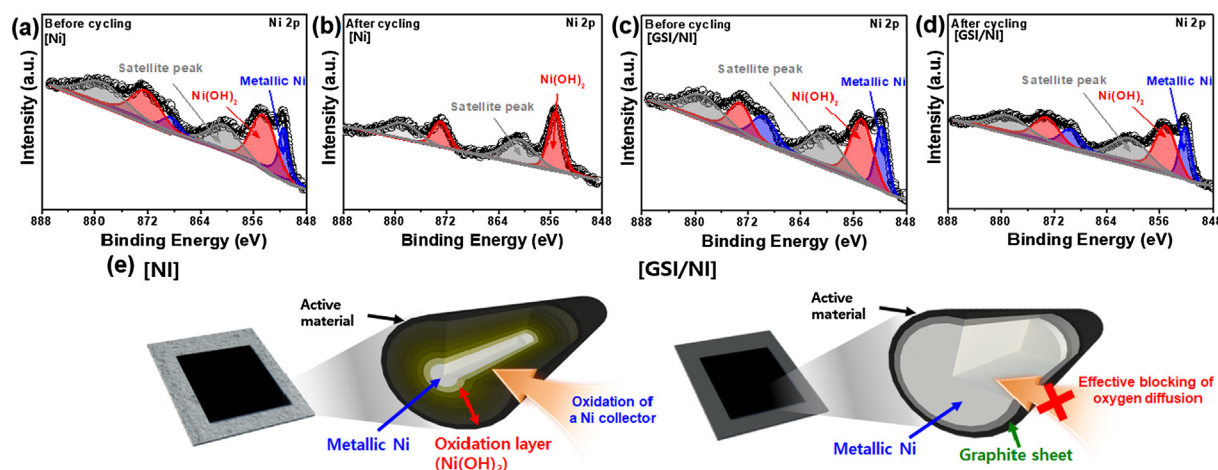


Fig. 7. XPS signals of Ni 2p for (a) NI before the cycling test; (b) NI after the cycling test; (c) GSI/NI before the cycling test; and (d) GSI/NI after the cycling test. Schematic illustration showing the electrochemical effects of interfacial phenomena in EDLCs after 10,000 cycles for (e) NI and (f) GSI/NI.

electrochemical features, the long-term cycling test was performed at the current density of  $1 \text{ A g}^{-1}$  after 10,000 cycles in the high-concentration of 8 M KOH electrolyte (see Fig. 6d). The triangular charging and discharging curves of GSI/NI exhibited linear slopes with a bilateral symmetry, suggesting ideal capacitance with high Coulombic efficiency (see the inset in Fig. 6d). GSI/NI showed excellent capacitance retention of 93%, whereas NI presented the poor capacitance retention of 67% with a rapid fading during 4000 cycles, which are much higher performance than those of the previously reported EDLCs (83% after 5000 cycles [31], 84% after 2000 cycles [32], 87% after 10,000 cycles [33], 91% after 10,000 cycles [34], and 92% after 3000 cycles [35]). For the reasons such as the corrosion of current collector, lead tap, and the packaging material the concentration of electrolyte has been limited so far in the 6 M KOH electrolyte [2–4]. Therefore, to overcome this problem, we suggested a novel design of the graphite nanosheet as an interlayer between the current collector and activated carbon.

Furthermore, to prove the role of the graphite nanosheet as interlayer, the X-ray photoelectron spectroscopy (XPS) measurement was performed before and after 10,000 cycling tests at the current density of  $1 \text{ A g}^{-1}$ . Fig. 7a–d shows XPS signals of Ni 2p for NI before the cycling test, NI after the cycling test, GSI/NI before the cycling test, and GSI/NI after the cycling test. XPS signals of Ni 2p were observed at 852.2 eV, 855.7 eV, and 862.1 eV, corresponding to metallic nickel, nickel hydroxide, and shake up satellites, respectively [36–40]. Before the cycling tests of NI and GSI/NI (see Fig. 7a and c), the nickel hydroxide could be ascribed to  $\text{O}_2$  and water vapor in the air [36–38]. In Fig. 7b, after 10,000 cycling tests, the extinction in the metallic Ni phase of NI, resulting from the oxidation reactions by high concentration electrolyte, can be observed. In detail, the metallic nickel phase was decreased from 37% to almost 0% after cycling test. By contrast, the metallic nickel phase of GSI/NI was almost maintained after the cycling test from 37% to 36% (see Fig. 7d). In addition, the durability of graphite nanosheet as an interlayer for GSI/NI was also preserved after the cycling test (see Figs. S6 and S7). Therefore, XPS results demonstrate that, in order to efficiently prevent the oxidation of the Ni, leading to the improved electrochemical performance (see Fig. 7e), the graphite nanosheet with its excellent chemical stability is a suitable candidate to be used as an interlayer between the current collector and activated carbon in EDLCs.

In sum, as expected, we assume that the remarkably enhanced energy storage performance of GSI/NI in the high-concentration electrolyte may be ascribed to the establishing a novel design of an interlayer as the graphite nanosheet. The large contact area between the current collector and activated carbon from the rough surface of the graphite nanosheet enables improved specific capacitance and outstanding high-

rate ability. Furthermore, the well-encapsulated graphite nanosheet prevents the oxidation of the Ni current collector, resulting in excellent cycling stability.

### 3. Conclusions

In the present study, we have suggested and designed an innovative concept of interface engineering between the current collector and activated carbon in EDLCs: a graphite nanosheet encapsulated on the Ni foam as the current collector provides synergistic effects to the electrical behavior and electrochemical stability. The excellent energy storage performance of GSI/NI in high-concentration electrolyte, as evidenced by a specific capacitance ( $236 \text{ F g}^{-1}$  at the current density of  $0.2 \text{ A g}^{-1}$ ), impressive high-rate ability of 87%, and remarkable cycling stability of 93% after 10,000 cycles were obtained. These improvements can be explained by the unique effect of a large contact area between the current collector and activated carbon from the graphite nanosheet as an interlayer. In addition, the well-encapsulated graphite nanosheet on the Ni foam facilitates prevention of the oxidation in high-concentration electrolyte, leading to an improvement of cycling stability. Taken together, the results of the present study convincingly demonstrate that interface engineering by the graphite nanosheet as an interlayer might be a powerful strategy not only for fundamental research on interfacial mechanisms in energy storage behavior, but also for realistic applications of EDLCs.

### Acknowledgments

This work was supported by the Technology Innovation Program (10080656, Development of ceramic/carbon convergence and integration anode material for 10C fast charging Lithium ion battery) funded By the Ministry of Trade, Industry & Energy (MOTIE, Korea).

### Appendix A. Supplementary material

Supplementary data to this article can be found online at <https://doi.org/10.1016/j.apsusc.2018.12.120>.

### References

- [1] C. Li, J. Balamurugan, N.H. Kim, J.H. Lee, *Adv. Energy Mater.* 8 (2018) 1702014.
- [2] P. Simon, Y. Gogotsi, *Nat. Mater.* 7 (2008) 845–854.
- [3] G. Wang, L. Zhang, J. Zhang, *Chem. Soc. Rev.* 41 (2012) 797–828.
- [4] P. Simon, Y. Gogotsi, B. Dunn, *Science* 343 (2014) 1210–1211.
- [5] G.-H. An, D.-Y. Lee, H.-J. Ahn, *J. Mater. Chem. A* 5 (2017) 19714–19720.
- [6] Y. Liu, Z. Zhou, S. Zhang, W. Luo, G. Zhang, *Appl. Surf. Sci.* 442 (2018) 711–719.
- [7] Y. Cheng, B. Li, Y. Huang, Y. Wang, J. Chen, D. Wei, Y. Feng, D. Jia, Y. Zhou, *Appl.*

- Surf. Sci. 439 (2018) 712–723.
- [8] D. Qu, X. Feng, X. Wei, L. Guo, H. Cai, H. Tang, Z. Xie, Appl. Surf. Sci. 413 (2017) 344–350.
- [9] G.-H. An, H.-J. Ahn, Carbon 65 (2013) 87–96.
- [10] C. Cai, Y. Zou, C. Xiang, H. Chu, S. Qiu, Q. Sui, F. Xu, L. Sun, A. Shah, Appl. Surf. Sci. 440 (2018) 47–54.
- [11] G.-H. An, B.-R. Koo, H.-J. Ahn, Phys. Chem. Chem. Phys. 18 (2016) 6587–6594.
- [12] Q. Xie, X. Huang, Y. Zhang, S. Wu, P. Zhao, Appl. Surf. Sci. 443 (2018) 412–420.
- [13] X. Xu, J. Gao, Q. Tian, X. Zhai, Y. Liu, Appl. Surf. Sci. 411 (2017) 170–176.
- [14] Y.-W. Lee, G.-H. An, B.-S. Kim, J. Hong, S. Pak, E.-H. Lee, Y. Cho, J. Lee, P. Giraud, S.N. Cha, H.-J. Ahn, J.I. Sohn, J.M. Kim, ACS Appl. Mater. Inter. 8 (2016) 17651–17658.
- [15] X.-L. Su, J.-R. Chen, G.-P. Zheng, J.-H. Yang, X.-X. Guan, P. Liu, X.-C. Zheng, Appl. Surf. Sci. 436 (2018) 327–336.
- [16] A.A. Silva, R.A. Pinheiro, A.C. Rodrigues, M.R. Baldan, V.J. Trava-Airoldi, E.J. Corat, Appl. Surf. Sci. 446 (2018) 201–208.
- [17] H. Ji, X. Zhao, Z. Qiao, J. Jung, Y. Zhu, Y. Lu, L.L. Zhang, A.H. MacDonald, R.S. Ruoff, Nat. Commun. 5 (2014) 3317.
- [18] D. Premathilake, R.A. Outlaw, R.A. Quinlan, S.G. Parler, S.M. Butler, J.R. Miller, J. Electrochem. Soc. 165 (2018) A924–A931.
- [19] P. Simon, Y. Gogotsi, Phil. Trans. R. Soc. A 368 (2010) 3457–3467.
- [20] C. Lei, F. Markoulidis, Z. Ashitaka, C. Lekakou, Electrochim. Acta 92 (2013) 183–187.
- [21] G.-H. An, H. Kim, H.-J. Ahn, ACS Appl. Mater. Inter. 10 (2018) 6235–6244.
- [22] G.-H. An, D.-Y. Lee, H.-J. Ahn, ACS Appl. Mater. Inter. 9 (2017) 12478–12485.
- [23] M. Guo, Y. Li, K. Du, C. Qiu, G. Dou, G. Zhang, Appl. Surf. Sci. 440 (2018) 606–613.
- [24] Z. Xu, Y. Li, D. Li, D. Wang, J. Zhao, Z. Wang, M.N. Banis, Y. Hu, H. Zhang, Appl. Surf. Sci. 444 (2018) 661–671.
- [25] K. Wu, Q. Liu, Appl. Surf. Sci. 379 (2016) 132–139.
- [26] J. Liang, T. Qu, X. Kun, Y. Zhang, S. Chen, Y.-C. Cao, M. Xie, X. Guo, Appl. Surf. Sci. 436 (2018) 934–940.
- [27] L. Pan, X. Li, Y. Wang, J. Liu, W. Tian, H. Ning, M. Wu, Appl. Surf. Sci. 444 (2018) 739–746.
- [28] Y. Yue, H. Liang, Small Methods 2 (2018) 1800056.
- [29] J.-Y. So, C.-H. Lee, J.-E. Kim, H.-J. Kim, J. Jun, W.-G. Bae, Materials 11 (2018) 1018.
- [30] H.R. Kim, W.M. Choi, Scr. Mater. 146 (2018) 100–104.
- [31] Ma, G. Wu, J. Wan, F. Ma, W. Geng, S. Song, RSC Adv. 5 (2015) 107785–107792.
- [32] G.-H. An, D.-Y. Lee, H.-J. Ahn, J. Ind. Eng. Chem. 65 (2018) 423–428.
- [33] K. Sun, S. Yu, Z. Hu, Z. Li, G. Lei, Q. Xiao, Y. Ding, Electrochim. Acta 231 (2017) 417–428.
- [34] C. Long, L. Jiang, X. Wu, Y. Jiang, D. Yang, C. Wang, T. Wei, Z. Fan, Carbon 93 (2015) 412–420.
- [35] K. Wang, N. Zhao, S. Lei, R. Yan, X. Tian, J. Wang, Y. Song, D. Xu, Q. Guo, L. Liu, Electrochim. Acta 166 (2015) 1–11.
- [36] S.H. Gage, C. Ngo, V. Molinari, M. Causà, R.M. Richards, F.S. Gentile, S. Pylypenko, D. Esposito, J. Phys. Chem. C. 122 (2018) 339–348.
- [37] M.K. Jeon, K.R. Lee, H.J. Jeon, P.J. McGinn, K.H. Kang, G.I. Park, Korean J. Chem. Eng. 32 (2015) 206–215.
- [38] G.-H. An, S.N. Cha, J.I. Sohn, Appl. Surf. Sci. 467–468 (2019) 1157–1160.
- [39] G.-H. An, H.-G. Jo, H.-J. Ahn, J. Alloys Compd. 763 (2018) 250–256.
- [40] G.-H. An, Y.-G. Lee, H.-J. Ahn, J. Alloys Compd. 746 (2018) 177–184.